Phys. Status Solidi A **208**, No. 11, 2522–2525 (2011) / **DOI** 10.1002/pssa.201184272

physica status solidi a
www.pss-a.com
applications and materials science

Coherent imaging at the Diamond beamline I13

Christoph Rau*[,1,2], Ulrich Wagner[1], Zoran Pešić[1], and Alberto De Fanis[1]

[1] Diamond Light Source Ltd., Chilton, Oxfordshire OX11 0DE, United Kingdom
[2] Northwestern University Feinberg School of Medicine, 303 E. Chicago Avenue, Searle 12-561, Chicago, IL 60611, USA

Received 28 November 2010, accepted 27 June 2011
Published online 28 October 2011

Keywords coherence, imaging, in-line phase contrast, microscopy, synchrotron

* Corresponding author: e-mail christoph.rau@diamond.ac.uk, Phone: +44 1235 778 796, Fax: +44 1235 778 448
Web: www.diamond.ac.uk

The Diamond beamline I13 for imaging and coherence applications is dedicated to hard X-ray imaging on the micro and nano-lengthscale. Two independent stations will be operated in a separate building at a distance of 250 m from the source. The imaging branch will perform in-line phase contrast imaging and tomography over a large field of view in the 6–35 keV energy range. In addition it will be possible to switch to full-field microscopy with 50 nm spatial resolution. Other microscopies will be developed according to the scientific needs. Resolution beyond the limitations given by the detector and X-ray optics will be achieved on the 'coherence' branch. Techniques working in the far field such as Coherent X-Ray Diffraction and other Coherent Diffraction Imaging techniques such as ptychography will be implemented. Typical applications cover different fields such as bio-medicine, materials science, geo- and astrophysics or even cultural heritage. The beamline hosts a number of innovative features such as the so-called 'mini-beta' layout for electron optics in the storage ring or new concepts for beamline instrumentation. The stations will be operational in 2011.

1 Introduction High-resolution imaging and tomography with synchrotron light has become well established for a large field of applications. The high penetration depth and partial coherence of the radiation permits imaging of weakly absorbing structures in opaque materials like soft tissue in a strong absorbing environment. Micrometer resolution over a relatively large field of view (millimeters) is achieved with a high resolution scintillation screens, coupled via a visible light microscope to a CCD chip. Nowadays available CMOS cameras allow imaging in the kHz regime for *in situ* studies. The variable photon energy from the synchrotron light provides access to more detailed chemical information. The spatial resolution has been recently improved with microscopes using highly efficient condenser optics (KB-mirror or capillary) in combination with high-resolution objective lenses (Fresnel zone plate) or in projection geometry. Spatial resolution beyond the limitations of X-ray optics and detectors can be achieved by imaging in reciprocal space, with different coherent diffraction imaging techniques. The spectrum of scientific applications at I13 will cover areas such as bio-medicine, materials sciences, or geo- and astrophysics [1]. For example for real-time imaging we plan the 'life' imaging of cochlear dynamics providing a deep insight into the hearing process [2]. On the coherence branch biological problems will also be studied, and perhaps even more interestingly these methods give access to internal information otherwise not accessible such as the internal stress in nano-crystals [3, 4].

2 Beamline layout Diamond is the latest UK based synchrotron of the 3rd generation, operating at 3 GeV energy. The beamline I13 is located in one of the long straight sections of the storage ring, providing space for two insertion devices (IDs). The vertical electron beam size at the location of the IDs can be significantly reduced by placing quadupole magnets in the centre of the straight section. As a result the undulator gap can be reduced to about 5 mm and hence the brilliance significantly increased, especially at higher photon energies. The difference in performance is shown in Fig. 1. This layout is called 'mini-beta' according to the small vertical beta functions in the sub-sections [5]. In each of the sections the horizontal beta function converges along the beam direction. For the second insertion device the waist of the electron and also the X-ray beam 11 m downstream. Close to this position (at 13 m) horizontal slits define the source size while the divergence remains unchanged. The horizontal coherence

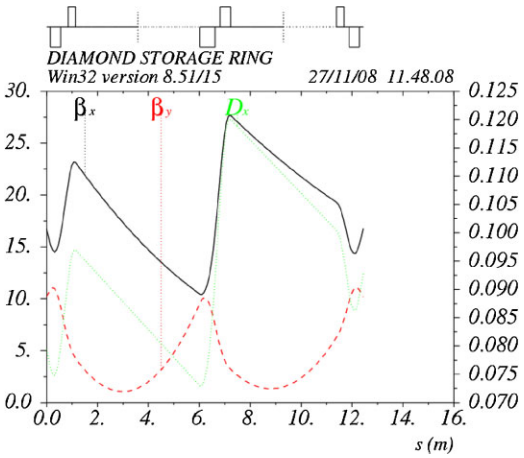

Figure 1 (online colour at: www.pss-a.com) Mini-beta layout. The quadrupole magnets (+, focusing; −, defocusing) in the centre cut the straight in two sections with low vertical beta values (β_y in red) which is proportional to the vertical beam size. In the second straight section the beam (β_x in black) focuses horizontally onto the front-end slits [5].

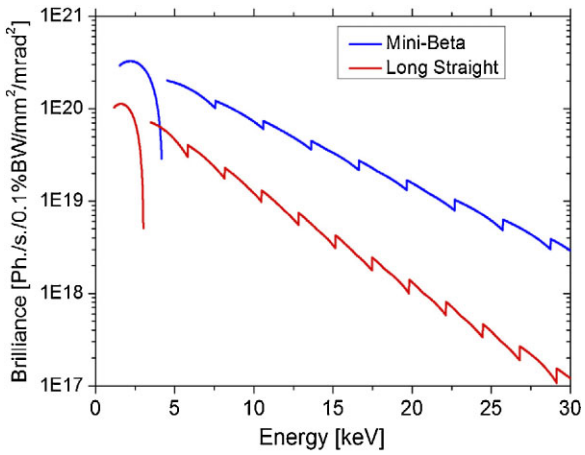

Figure 2 (online colour at: www.pss-a.com) Performance of 3 m long U20 cryo-cooled undulator (blue) for the coherence branch. For comparison in red the performance of a comparable undulator in a long straight (U28).

length can be varied over a large range and matched to the value in the vertical direction. This layout allows for a 2 m long undulator (Fig. 2) to be operated with 5 mm gap and a 2.8 m long device with 6.3 mm gap. They are canted by 4 mrad to each other so that both branches will be operated independently (scheme Fig. 3a). The new electron optics is currently used in normal operation mode of the storage ring, maintaining source size and stability for all other beamlines. Some parameters provided in the following for the photon beam may be still further adapted.

3 The branches In the coherence branch, the divergence of the X-ray beam is 50 μrad × 25 μrad and its minimal size is about 400 μm × 13 μm (horizontal × vertical; all FWHM). The vertical minimum is located in

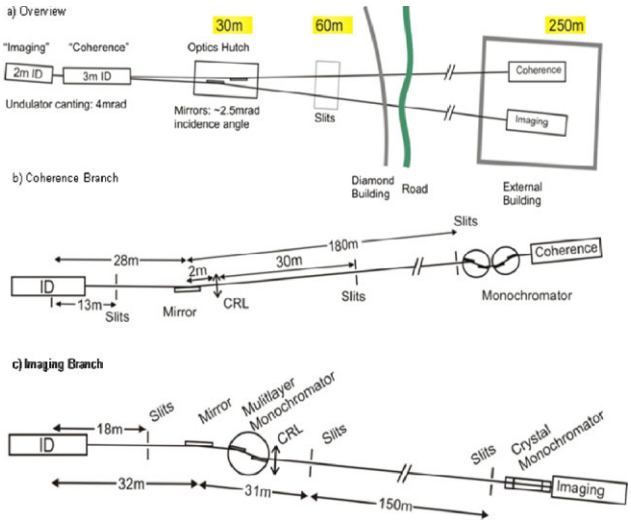

Figure 3 (online colour at: www.pss-a.com) Layout of the branches at I13.

the centre of the undulator, the horizontal minimum is 11 m further downstream. The insertion device is expected to provide a flux of 7×10^{14} Ph/s/0.1% BW and a coherent flux of about 10^{10} Ph/s/0.1% BW at 8 keV, which is the optimal working energy. From the centre of the insertion device the front-end slits are placed about 13 m downstream (see Fig. 3b). The deflecting optics further downstream (mirror, monochromator) are placed horizontally to minimise eventual deterioration of the coherent flux [6]. Water cooling is chosen for optimal stability. The flat mirror at 28 m distance has a deflection angle of 4.6 mrad with Si, Rd and Pt stripes for different cut-off energies. The surface is super polished over a small area reaching a slope error less than 170 nrad. The crystal shape is designed to compensate for possible surface deformation under heatload [7]. The monochromator is in the external building, at about 210 m, using pseudo- channel-cut crystals. The four-bounce design provides fixed-exit at all energies and beam collimation. The longitudinal coherence length can be modified by detuning the crystal pairs to each other or selecting between a Si(111) and Si(311) set. Slits just in front of this monochromator define the beam divergence. Lenses at 30 m can be inserted to the beam for collimation or generating an intermediate (vertical) focus at about 60 m. In the vertical direction, the coherence lengths can be adapted over a large range, and in combination with slits placed at the 60 m position, the source position is fixed with high stability. In the horizontal direction, beam position and source size is defined by the front-end slits. Some filters can be inserted in the beam to reduce heat load on optics.

The imaging branch operates at photon energies of about 20 keV and above. The flux at that energy will be 10^{14}/s/0.1% BW. Similar to the coherence branch, slits are in the front end and a mirror with several stripes is in the optical hutch as the first major component (see Fig. 3c). The mirror can be bent horizontally. Behind the mirror, a multilayer monochromator is placed for fast imaging applications using a large

bandwidth. In the external hutch a water-cooled double-crystal monochromator is used for absorption contrast experiments. Focusing lenses can be inserted to customize the beam size. Without using the focusing optics, the beam size in the external hutch is about $12 \times 6\,\mathrm{mm}^2$ ($h \times v$) (all FWHM).

4 The experimental stations For both branches the experimental floor is completely isolated from the building. Between hall floor, the concrete walls of the hutches and the experimental floor plate is a gap, the experimental floor plate is placed on concrete piles. Other peripheral such as air conditioning is isolated from the hutch, too. The stability of the experimental floor in respect to the Diamond ring building is recorded with an autocollimator and a hydrostatic levelling system. Although the dimensions for both experimental hutches are similar (17 m and 23 m) the process underlying the image formation process are fundamentally different.

4.1 The imaging stations The imaging station is dedicated to micro- and nano-imaging with resolution up to 50 nm. In-line phase contrast imaging will be performed in the energy range of 8–35 keV, the field of view can be adapted between 1 and $20\,\mathrm{mm}^2$ (scheme Fig. 4, top). In-line phase contrast imaging relies on the enhancement of the contrast on the edges of weakly absorbing objects when using partial coherent light. The setup consists of a sample and detector stage placed on a vibration isolated table. The distance between both can be freely changed, modulating the edge enhanced contrast in the radiograph. The spatial resolution depends on the detector system. The X-ray active layer of a scintillation screen transforms the X-rays into visible light. This image is then projected through a microscope optic, adapted to the screen on the chip of the CCD camera. Faster recording is achieved with cameras using CMOS technology. It is expected to achieve micrometer resolution and exposure times less than 10 ms and with 10 μm resolution 0.1 ms. One application planned for this type of experiments is for example the dynamic study of micromechanics in mammal cochlear. Adapted sample environments can be installed on separate experimental tables. It will be for example possible to study samples under stress, pressure and at high or low temperatures. In addition imaging and tomography with chemical speciation will be made available. The oxidation state of different sample constituents can be resolved with some microns resolution.

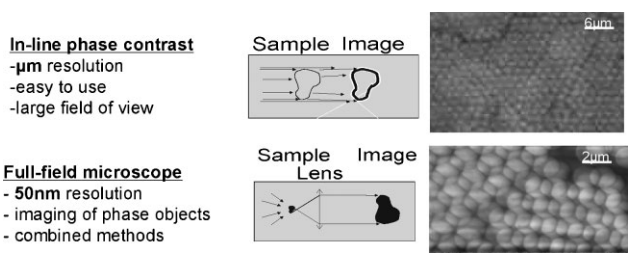

Figure 4 Schematic representation of imaging methods available at I13.

For example the electro-chemical process in fuel cells can be studied.

Improved spatial resolution is achieved by swapping a hard X-ray microscope into the experimental setup (scheme Fig. 4, bottom). Similar to a visible light microscope its main components are the condenser optic and the objective lens. The highly efficient condenser optic (a KB-mirror or similar) is matched to the objective lens aperture. For the latter a Fresnel-zone plate (FZP) provides the high spatial resolution. A FZP with 40 nm outermost zone width provides 50 nm spatial resolution. Again, the field of view can be varied by scanning the condenser optic, the expose times is about a second for a $20 \times 20\,\mu\mathrm{m}^2$ field of view. A phase ring and other beam defining elements are moved into the beam for Zernike phase contrast imaging. The details of the instrument are described elsewhere [8, 9].

Other instrumental developments will have the goal to make more use of phase information and to increase the dose efficiency, namely grating interferometer and cone-beam imaging. More details can be found elsewhere [10] and are not object of the present paper.

4.2 The coherence station The coherence station is dedicated for imaging with highest achievable resolution. For coherent X-ray diffraction (CXRD) and coherent diffraction imaging (CDI) the achievable resolution is neither limited by the detector nor by the X-ray optics. Under coherent illumination the sample produces a diffraction pattern at large distances (far field). Original structure and pattern are related through Fourier transformation and the object is reconstructed through iterative methods. For this type of experiments the beam size is reduced in the experimental hutch to the coherent fraction and focused with either a zone plate or KB optic onto the sample [11]. The coherence length and therefore the illuminated field can be modified over a large range from some to a couple of hundred microns and can be further increased by scanning the focussing optic. The entire object is reconstructed then by a technique known in literature as 'ptychography'. The sample itself can be tilted and rotated with a goniometer setup. Again variable sample environment will be made available. For CXRD experiments the detector will be held on a robotic arm, providing a position stability of some microns. A photon counting detector system based on the MediPix chip is currently under development (see also [14]). It covers a $1.5\,\mathrm{k} \times 2\,\mathrm{k}$ array with 55 microns pixel size. In forward direction for coherent diffraction imaging the detector will be installed on a rail and can be translated up to 19 m from the sample away (scheme Fig. 5).

Some innovations to these experiments are planned to be implemented. Recently the combination of CXRD and full-field microscopy has been tested on a $BaTiO_3$ sample, where data from both can be combined for reconstruction. Other imaging methods mentioned above may be used for rather measuring than iterative guessing of the phase information.

Very high temporal resolution is achieved in photo-correlation spectroscopy, using a very similar experimental

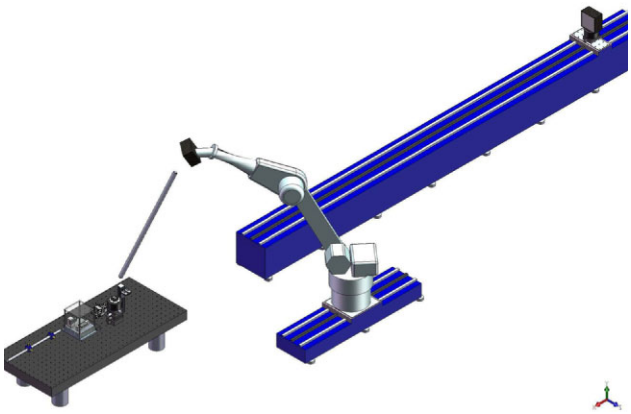

Figure 5 (online colour at: www.pss-a.com) Experimental setup for the coherence branch at I13. A robotic arm [12, 13] will be used for supporting the detector.

setup compared to CDI. Here the goal is much less to measure the structure of objects rather than the time correlation between them. This type of study is in particular of interest for low viscosity liquids such as polymers or glasses.

5 Summary I13 is a 250 m long beamline for imaging and coherence applications. It covers the energy range between 6–35 keV for studies on the micro- and nano-lengthscale. Two independent stations operate in reciprocal and real space to cover different high-resolution techniques. The beamline layout takes into account the high requirements for stability of the beamline. Modifications of the storage ring optics (mini-beta) allow high brilliance and matching of the lateral coherence lengths.

Acknowledgements I. K. Robinson is acknowledged for discussions. The imaging branch at I13 is funded in conjunction with the University of Manchester. Further the I13 engineering team is greatly acknowledged, in particular A. Peach and G. Wilkin.

References

[1] http://www.diamond.ac.uk/beamlines/I13L.
[2] C. Rau, I. K. Robinson, and C. P. Richter, Microsc. Res. Technol. **69**(8), 660–665 (2006).
[3] I. K. Robinson and R. Harder, Nature Mater. **8**, 291–298 (2009).
[4] R. Harder, M. A. Pfeifer, G. J. Williams, I. A. Vartaniants, and I. K. Robinson, Phys. Rev. B **76**(11), 115425 (2007).
[5] B. Singh, R. Bartolini, R. Fielder, E. C. Longhi, I. P. Martin, U. H. Wagner, and C. Rau, in: 23rd Particle Accelerator Conference (Vancouver, Canada, 2010), pp. 1–3.
[6] U. H. Wagner and C. Rau, in: 10th International Conference on Synchrotron Radiation Instrumentation (Melbourne, Australia, 2010), pp. 461–464.
[7] A. M. Khounsary, in: Conference on X-Ray Optics Design, Performance, and Applications (Denver, CO, USA, 1999), p. 78.
[8] C. Rau, V. Crecea, W. Liu, C.-P. Richter, K. M. Peterson, P. R. Jemian, U. Neuhäusler, G. Schneider, X. Yu, P. V. Braun, T. V. Chiang, and I. K. Robinson, Nucl. Instrum. Methods Phys. Res. B **261**(1–2), 850–854 (2007).
[9] C. Rau, V. Crecea, C.-P. Richter, K. M. Peterson, P. R. Jemian, U. Neuhäusler, G. Schneider, X. Yu, P. V. Braun, T.-C. Chiang, and I. K. Robinson, Micro Nano Lett. **2**, 1–5 (2007).
[10] C.-P. Richter, S. Shintani-Smith, A. Fishman, C. David, I. K. Robinson, and C. Rau, Microsc. Res. Technol. **72**(12), 902–907 (2009).
[11] I. K. Robinson, F. Pfeiffer, I. Vartanyants, Y. Sun, and Y. Xia, Opt. Express **11**(19), 2329–2334 (2003).
[12] D. Shu, J. Maser, M. Holt, R. Winarski, C. Preissner, B. Lai, S. Vogt, and G. B. Stephenson, Nucl. Instrum. Methods Phys. Res. **582**(1), 159–161 (2007).
[13] Z. D. Pešić, U. H. Wagner, and C. Rau, in: 7th International Conference on Synchrotron Radiation in Materials Science (Cambridge University Press, Oxford, UK, 2010), p. e103.
[14] N. Tartoni, I. C. Horswell, J. Marchal, E. N. Gimenez, R. D. Fearn, and R. G. van Silfhout, in: 10th International Conference on Synchrotron Radiation Instrumentation (Melbourne, Australia, 2010), pp. 851–855.